J Mater Sci: Mater Electron (2016) 27:425–435
DOI 10.1007/s10854-015-3770-0

Preparation and characterization of $BaSnO_3$ nanostructures via a new simple surfactant-free route

Saeed Moshtaghi[1] · Sahar Zinatloo-Ajabshir[1] · Masoud Salavati-Niasari[1]

Received: 23 July 2015 / Accepted: 7 September 2015 / Published online: 11 September 2015
© Springer Science+Business Media New York 2015

Abstract Pure barium stannate ($BaSnO_3$) nanostructures were prepared via a new facile surfactant-free coprecipitation-calcination route by employing $Ba(Sal)_2$ (Sal = salicylidene) and $SnCl_2{\cdot}2H_2O$ as precursors. $Ba(Sal)_2$ was employed as precursor to synthesize $BaSnO_3$ nanostructures for the first time. The as-obtained $BaSnO_3$ nanostructures were analyzed by UV–vis diffuse reflectance spectroscopy, field emission scanning electron microscopy, Fourier transform infrared spectroscopy, energy dispersive X-ray microanalysis, transmission electron microscopy, and X-ray diffraction. Based on the morphological investigations of the as-prepared samples, it was found that the particle size and shape of the $BaSnO_3$ depended on the reaction temperature, precipitator and surfactant. $BaSnO_3$ nanostructures with various shapes and particle sizes were successfully prepared. Furthermore, the photocatalytic properties of as-synthesized $BaSnO_3$ were evaluated by degradation of eriochrome black T (anionic dye) as water contaminant.

1 Introduction

Research on preparation and characterization of nanostructured materials is well-known as a significant field in recent science and technology [1–5]. One of these nanostructured materials is barium stannate ($BaSnO_3$). Barium stannate as one of the most attractive alkaline earth stannates is well-known for its excellent potential applications, including protective coating, capacitors, catalyst support, photocatalyst, ceramic and sensor [6–12] as well as remarkable and specific dielectric, optical, photovoltaic, and electrical properties [7, 13, 14]. $BaSnO_3$ with perovskite structure has cubic crystal form [15]. Until now, solid state [16], combustion [17], sol–gel [18], reverse micelle [19] and coprecipitation [20] process have been introduced for the preparation of $BaSnO_3$. It is generally accepted that the particle size and shape have important impact on the behavior of nanostructured materials, and therefore they play key and significant role in the final application of nanostructured materials. So, different preparation methods have been exploring to control the particle size and shape of nanostructured materials [21–23].

It has been shown that inorganic or organometallic compounds with special and interesting architecture can be employed as starting materials to prepare nanostructured materials and controlling their size and shape [21–24].

This work describes a new facile coprecipitation-calcination procedure to prepare $BaSnO_3$ nanostructures with the aid of $Ba(Sal)_2$ (Sal = salicylidene) and $SnCl_2{\cdot}2H_2O$ as precursors. The synthesis of many inorganic nanostructured materials by coprecipitation–calcination procedure as a favorable, reliable, simple and effective synthetic way becomes increasingly significant owing to the easy control of the purity, particle size and shape. To our knowledge, it is the first time that $Ba(Sal)_2$ (Sal = salicylidene) is utilized as barium source for the synthesis of $BaSnO_3$ nanostructures and the effects of critical preparation factors on the size and shape of the $BaSnO_3$ via a new simple surfactant-free coprecipitation-calcination process are studied.

✉ Masoud Salavati-Niasari
salavati@kashanu.ac.ir

[1] Institute of Nano Science and Nano Technology, University of Kashan, P. O. Box 87317-51167, Kashan, I. R. Iran

2 Experimental

2.1 Materials and characterization

All the chemicals employed for the preparation of $BaSnO_3$ nanostructures including $SnCl_2{\cdot}2H_2O$, methanol, $Ba(NO_3)_2$, salicylaldehyde (Sal), ethylenediaminetetraacetic acid disodium salt (Titriplex III), tetraethylenepentamine (TEPA), ethylenediamine (EN), triethylenetetramine (Trien) and sodium dodecyl sulphate (SDS) were purchased from Merck Company and were utilized as received. The energy dispersive spectrometry (EDS) analysis was examined by Tescan mira3 microscope. Powder X-ray diffraction (XRD) patterns of as-obtained samples were collected from a Philips diffractometer applying X'PertPro and the monochromatized Cu Ka radiation (l = 1.54 Å). The UV–vis diffuse reflectance spectra of the as-synthesized $BaSnO_3$ nanostructures were obtained on a UV–vis spectrophotometer (Shimadzu, UV-2550, Japan). FE-SEM images of the $BaSnO_3$ samples were obtained on Hitachi S-4160 field emission scanning electron microscope (FESEM). Fourier transform infrared spectra of the as-prepared products were obtained employing KBr pellets on an FT-IR spectrometer (Magna-IR, 550 Nicolet) in the 400–4000 cm^{-1} range. Transmission electron microscope (TEM) micrographs of $BaSnO_3$ nanostructures were obtained on a JEM-2100 with an accelerating voltage of 200 kV equipped with a high resolution CCD Camera.

2.2 Synthesis of $Ba(Sal)_2$

To synthesize $Ba(Sal)_2$, a salicylaldehyde solution (6 mmol in 60 mL of methanol) was added drop-wise to an aqueous $Ba(NO_3)_2$ solution (3 mmol in 60 mL of distilled water) under magnetic stirring. The $Ba(Sal)_2$ was obtained after refluxing the mixture for about 3 h.

2.3 Synthesis of $BaSnO_3$ nanostructures

$BaSnO_3$ nanostructures were synthesized by novel coprecipitation-calcination way. In a typical experiment, 1 mmol of $Ba(Sal)_2$ and 1 mmol of $SnCl_2{\cdot}2H_2O$ were dissolved in 30 mL hot distilled water (60 °C) separately. $SnCl_2{\cdot}2H_2O$ solution was added into a solution of $Ba(Sal)_2$ drop-wise under magnetic stirring. The pH of the resultant solution was adjusted to 13 by adding EN solution drop-wise and final solution was heated at 60 °C for 1 h under constant stirring. The yellow precipitate was filtered, washed out with distilled water for three times, air-dried and calcined at 700 °C for 4 h (sample no. 1). Schematic diagram of the synthesis of the $BaSnO_3$ nanostructures is illustrated in Scheme 1. To examine the surfactant influence, a stoichiometric amount of the surfactant was dissolved in 4 mL distilled water and added after mixing $SnCl_2{\cdot}2H_2O$ and $Ba(Sal)_2$ solutions. The influence of the reaction temperature, precipitator and surfactant on the particle size and shape of the $BaSnO_3$ were investigated and the obtained results illustrated in Table 1.

2.4 Photocatalytic test

The photocatalytic characteristics of as-prepared $BaSnO_3$ nanostructures were evaluated by utilizing eriochrome black T (anionic dye) solution. The Solution including 0.001 g of the eriochrome black T and 0.004 g of the as-synthesized $BaSnO_3$ in the quartz reactor was utilized to carry out the photocatalytic test. After aerating for 30 min, the mixture was subjected to the irradiation of the UV light from the 400 W mercury lamps. The eriochrome black T photodegradation percentage was estimated as follow:

$$D.P.\,(t) = \frac{A_0 - A_t}{A_0} \times 100 \qquad (1)$$

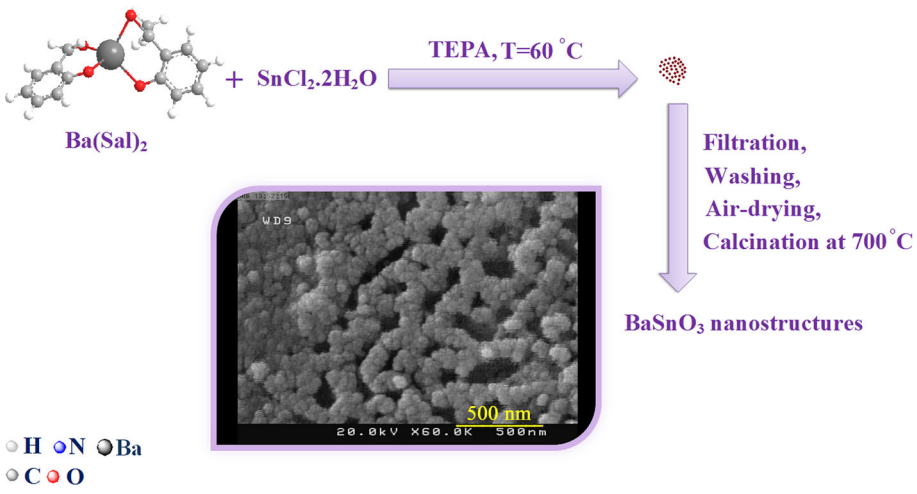

Scheme 1 Schematic diagram of the preparation of the $BaSnO_3$ nanostructures

Table 1 The reaction conditions for synthesis of the $BaSnO_3$ micro/nanostructures

Sample no.	Precipitator	Precursors	Surfactant	Reaction temperature (°C)	Figure of SEM images
1	EN	$Ba(Sal)_2$ and $SnCl_2{\cdot}2H_2O$	–	60	4a
2	Trien	$Ba(Sal)_2$ and $SnCl_2{\cdot}2H_2O$	–	60	4b
3	TEPA	$Ba(Sal)_2$ and $SnCl_2{\cdot}2H_2O$	–	60	4c
4	TEPA	$SnCl_2{\cdot}2H_2O$	–	60	5a
5	TEPA	$Ba(Sal)_2$	–	60	5b
6	TEPA	$Ba(Sal)_2$ and $SnCl_2{\cdot}2H_2O$	–	25	7a
7	TEPA	$Ba(Sal)_2$ and $SnCl_2{\cdot}2H_2O$	–	90	7b
8	TEPA	$Ba(Sal)_2$ and $SnCl_2{\cdot}2H_2O$	SDS	60	8a
9	TEPA	$Ba(Sal)_2$ and $SnCl_2{\cdot}2H_2O$	Titriplex III	60	8b
10[a]	TEPA	$Ba(NO_3)_2$ and $SnCl_2{\cdot}2H_2O$	–	60	9a

[a] Blank test

where A_t and A_0 are the obtained absorbance value of the eriochrome black T solution at t and 0 min by a UV–vis spectrometer, respectively.

3 Results and discussion

It has been shown that FT-IR spectroscopy is desirable and suitable device for understanding the functional group of any organic compound. The infrared spectra of the $Ba(Sal)_2$ and sample no. 3 after washing steps and after calcination are illustrated in Fig. 1a–c. In the FT-IR spectrum of the $Ba(Sal)_2$ (Fig. 1a), the bands located at 1524 and 1637 cm^{-1} are corresponding to the C–O stretching vibrations and the band centered at 1434 cm^{-1} is corresponding to the C–C stretching vibration of the Sal compound. The C–O stretching vibrations and C–C stretching vibration of the free Sal compound appears at 1680 and 1660 cm^{-1} as well as at 1490 cm^{-1}. Upon $Ba(Sal)_2$ preparation, these vibrations shifted to lower regions [25]. The absorption peak located at 3306 cm^{-1} in the FT-IR spectrum of the $Ba(Sal)_2$ is corresponding to the stretching vibrations of the physisorbed water molecules. Absorption peak at 466 cm^{-1} may correspond to Ba–O band, there is no peak nearby this point in Sal compound. The peaks located at 856 and 1449 cm^{-1} in Fig. 1b can be related to carbonate group [20]. Besides the peak seen at 550 cm^{-1} may be related to the Sn–O stretching vibration [26]. In the case $BaSnO_3$ nanostructures (sample no. 3 after calcination), the absorption peak seen at 3425 cm^{-1} are corresponding to the ν(OH) stretching vibration of the surface adsorbed water molecules [22]. The characteristic peak of the $BaSnO_3$ located at 645 cm^{-1} [27] (Fig. 1c).

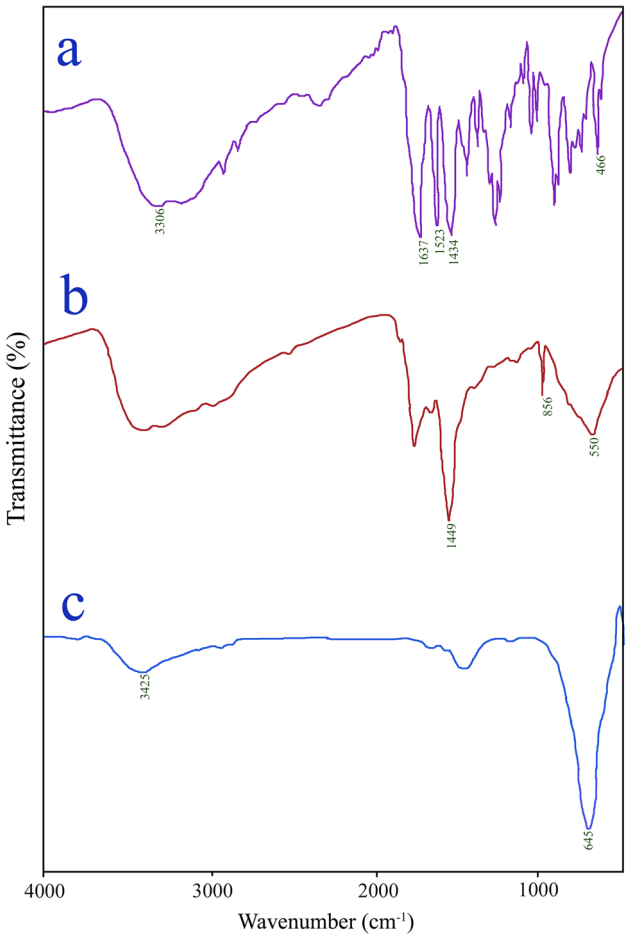

Fig. 1 FT-IR spectra of $Ba(Sal)_2$ (*a*), sample no. 3 after washing (*b*), and after calcinacion (*c*)

To determine the crystal structure, composition and mean crystallite diameter of the as-obtained samples, XRD analysis was performed. Figure 2a, b exhibits XRD

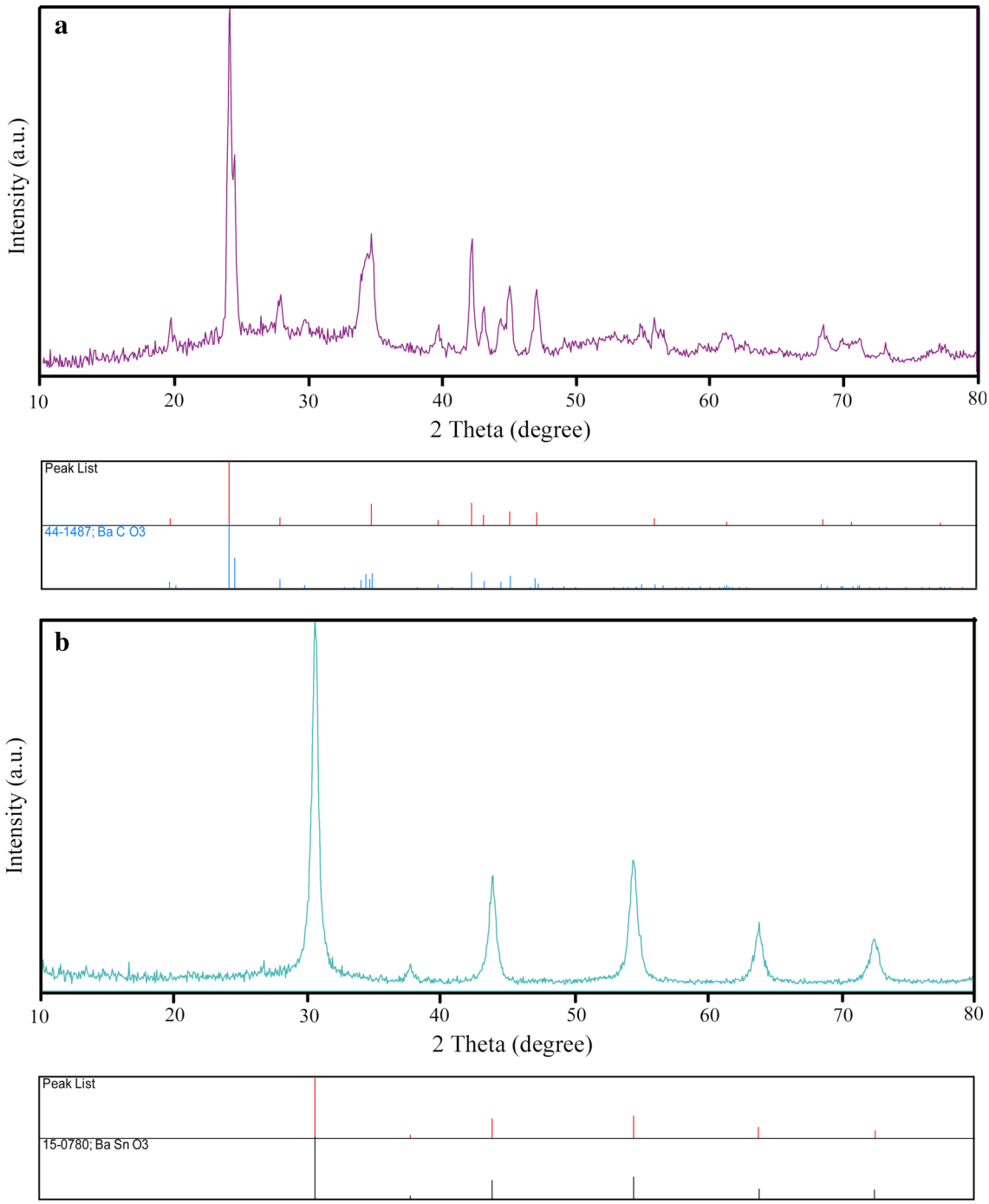

Fig. 2 XRD patterns of the sample no. 3 after washing (**a**), and after calcinacion (**b**)

patterns of the sample no. 3 after washing steps and after calcination, respectively. All of the diffraction peaks observed in Fig. 2a can be indexed to orthorhombic $BaCO_3$ with space group of Fd3 m (JCPDS card 44-1487). FT-IR and XRD results (Figs. 1b, 2a) demonstrate that the precipitate formed at the coprecipitation procedure containing $BaCO_3$ and $Sn(OH)_2$ (after washing steps). It seems that the separated Ba^2+ ions from $Ba(Sal)_2$ in the basic condition (pH 13) has high affinity to the atmospheric CO_2, thus $BaCO_3$ phase forms [27]. Besides, $Sn(OH)_2$ is amorphous and therefore, no its diffraction peaks appears in Fig. 2a. All the diffraction

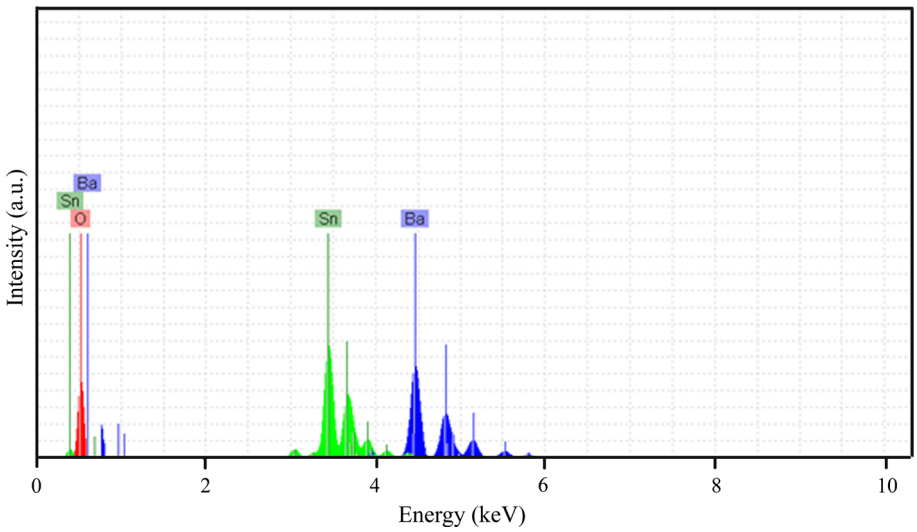

Fig. 3 EDS pattern of $BaSnO_3$ nanostructures (sample no. 3)

peaks in XRD pattern of the sample no. 3 after calcination can be indexed to pure cubic $BaSnO_3$ with Pm-3 m space group (JCPDS 15-0780). No impurities are illustrated in this pattern. Utilizing Scherrer formula [22], the mean crystallite size of the prepared $BaSnO_3$ nanostructures (sample no. 3) from the XRD results was estimated to be about 20 nm.

In order to study the purity level and chemical composition of the as-synthesized $BaSnO_3$ nanostructures (sample no. 3), EDS technique was employed. Figure 3 reveals the EDS spectrum of the sample no. 3. The EDS spectrum demonstrates that this sample containing Ba, Sn and O elements. So, the EDS and XRD results confirm the high purity of the as-obtained $BaSnO_3$ nanostructures.

FESEM technique was applied to examine the effects of the critical preparation factors on the size and shape of the $BaSnO_3$. The precipitator sort effect on the particle size and shape of the $BaSnO_3$ was investigated (Fig. 4a–c). For this propose, the reactions were performed in presence of the EN, Trien and TEPA (sample nos. 1–3). The FESEM images demonstrate that irregular micro/nanostructures, not uniform sphere-like nanostructures and uniform spherical nanoparticles are prepared in the presence of the EN, Trien and TEPA, respectively. Among these applied precipitator sorts, TEPA has the highest steric hindrance influence (Scheme 2). TEPA can play as both precipitator and co-capping agent role and hinder from the aggregation of the formed nanoparticles. Furthermore, FESEM images illustrate that the increase in the steric hindrance influence causes the grain size becomes small. It seems that the nucleation to be happened rather than the particle growth by increasing the steric hindrance influence. It can be deduced that TEPA was the best precipitator sort for $BaSnO_3$ nanoparticles with uniform spherical shape and small grain size (Fig. 4c).

To examine the effect of the presence of Ba and Sn on the shape and particle size of the products, two reactions was carried out in the absence of Ba and Sn. Figure 5 exhibits the FESEM images of the sample nos. 4 and 5 prepared in the absence of Ba and Sn, respectively. From the FESEM images, it can be observed that bulk structures decorated by not uniform nanoparticles and high agglomerated particles/bulk structures are obtained in the absence of Ba and Sn, respectively (Fig. 5a, b). According to the XRD results illustrated in Fig. 6, $BaCO_3$ and SnO_2 are prepared in the absence of Sn and Ba. The proposed formation mechanism of $BaSnO_3$ nanostructures employing $Ba(Sal)_2$ (Sal = salicylidene) and $SnCl_2{\cdot}2H_2O$ in the presence of TEPA can be summarized as follows:

$$Ba(C_6H_4(CHO)O)_2 \rightarrow Ba^{2+} + 2C_6H_4(CHO)O^-$$

$$SnCl_2 + 2H_2O \rightarrow Sn(OH)_2 + 2H^+ + 2Cl^-$$

$$2C_6H_4(CHO)O^- + 2H^+ \rightarrow 2C_6H_4(CHO)OH$$

$$Ba^{2+} + CO_2 + 2OH^- \rightarrow BaCO_3 + H_2O$$

By calcining the precipitate formed at the coprecipitation procedure containing $BaCO_3$ and $Sn(OH)_2$, at 700 °C for 4 h, the pure cubic $BaSnO_3$ nanostructures prepare as follows [27]:

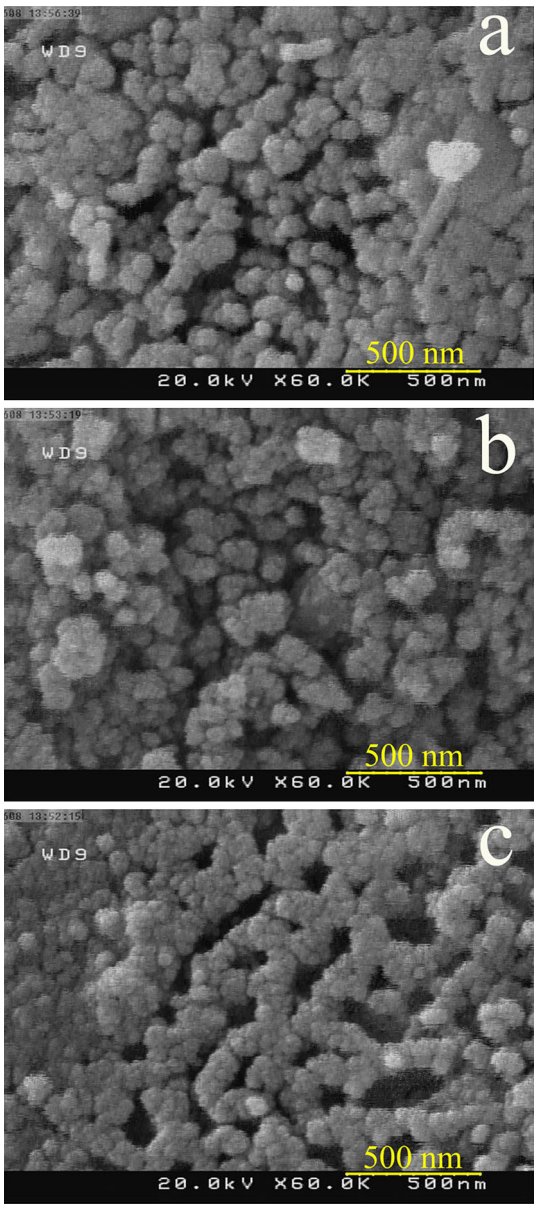

Fig. 4 FESEM images of the samples synthesized by **a** EN, **b** Trien and **c** TEPA

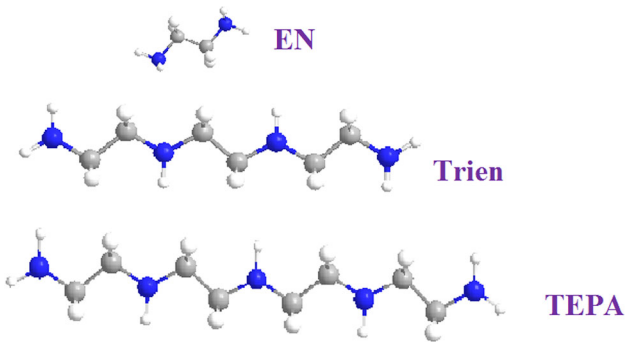

Scheme 2 Three different amines used as precipitator

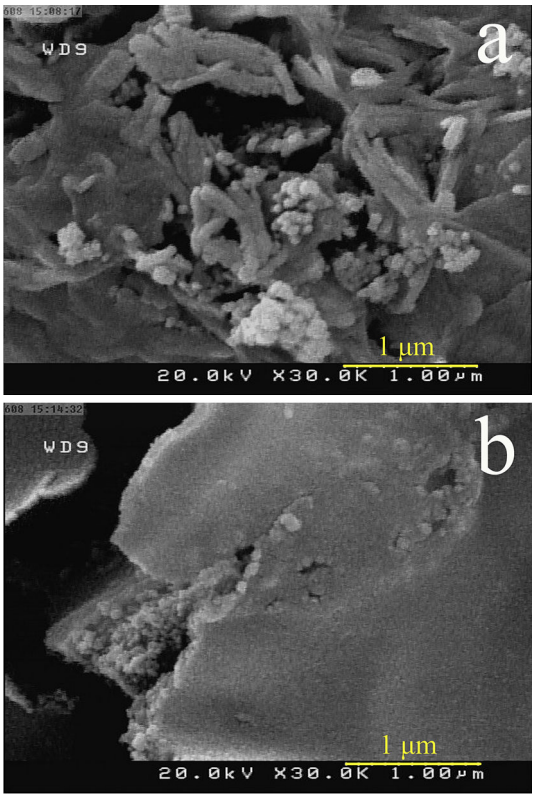

Fig. 5 FESEM images of the samples synthesized in the absence of **a** Ba and **b** Sn

$$Sn(OH)_2 + O_2 \rightarrow 2SnO_2 + 2H_2O$$
$$BaCO_3 + SnO_2 \rightarrow BaSnO_3 + CO_2$$

The obtained FT-IR and XRD results (Figs. 1, 2, 6) confirm this proposed mechanism for $BaSnO_3$ nanostructures formation.

The reaction temperature influence on the shape and size of the $BaSnO_3$ was also examined (Fig. 7). For this aim, two samples were prepared at 25 and 90 °C (sample nos. 6 and 7). The shape of the sample no. 6 in Fig. 7a is not uniform sphere-like. The sample no. 7 formed at 90 °C illustrates high agglomerated particle-like structures (Fig. 7b). It can be observed that with the reaction temperature change from 60 to 25 °C, the grain size increases. It is generally accepted that the enhancement of the reaction temperature always causes an enhancement of the rate of the reaction. Thus by performing the reaction at relatively high temperature more $BaSnO_3$ nuclei will obtain before the growth step, which results in the preparation of more particles with smaller sizes. By changing the temperature from 60 to 90 °C (Fig. 7b), the particles

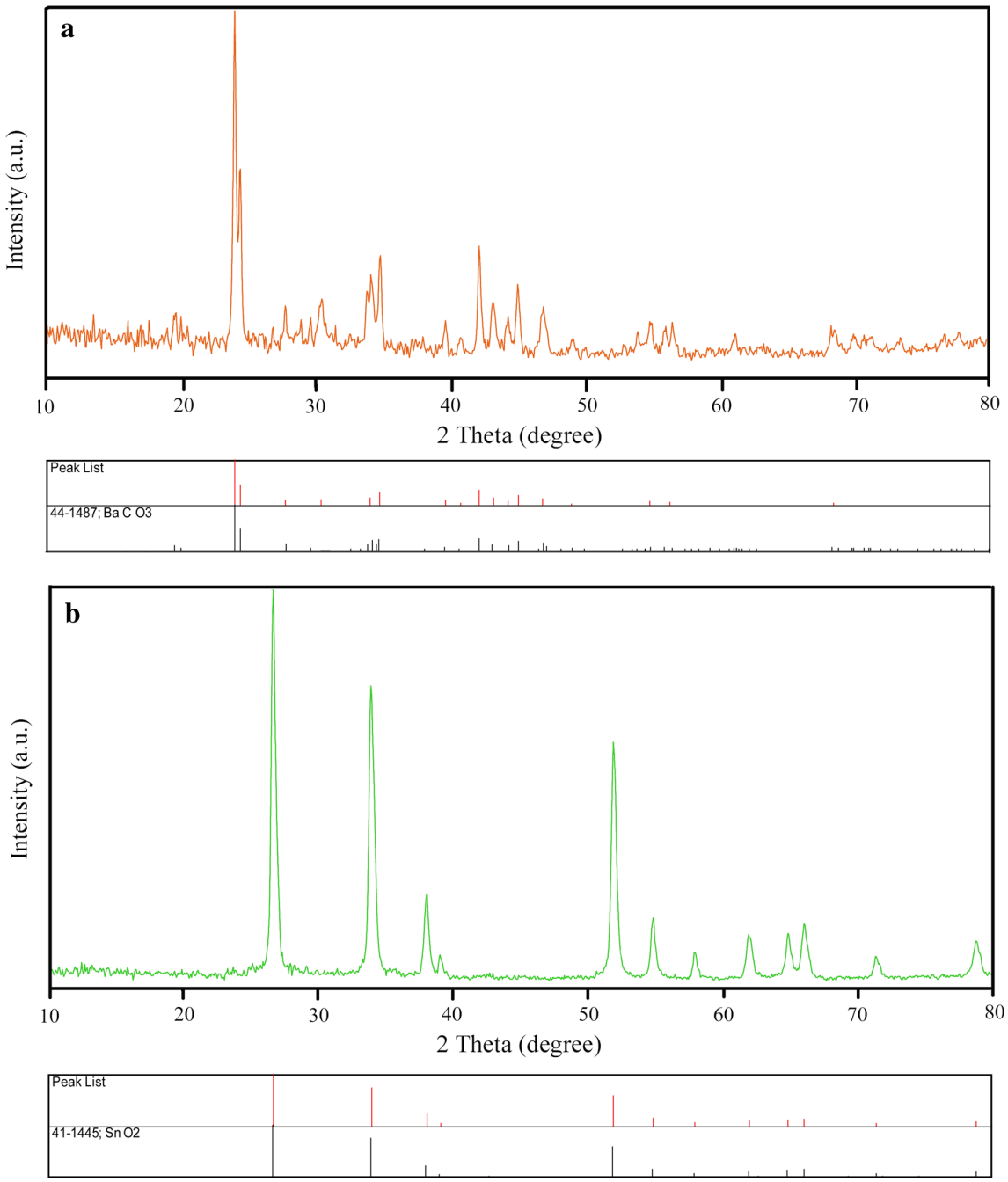

Fig. 6 XRD patterns of the samples prepared in the absence of **a** Ba and **b** Sn

agglomeration enhanced and the grain size decreased. According to the FESEM results, the most favorable reaction temperature for uniform spherical nanoparticles preparation is 60 °C temperature.

In continuation, the influence of the surfactant sort on the shape and size was examined (Fig. 8). To study the effect of this factor, two reactions were performed in presence of the SDS and Titriplex III (sample nos. 8 and 9). The sample nos. 8 and 9 illustrate not uniform sphere-like nanostructures and irregular bulk structures, respectively (Fig. 8a, b). The obtained results demonstrated that employing these surfactant types not only is favorable and advantageous to form product with a regular and uniform morphology, but also causes to prepare the inhomogeneous

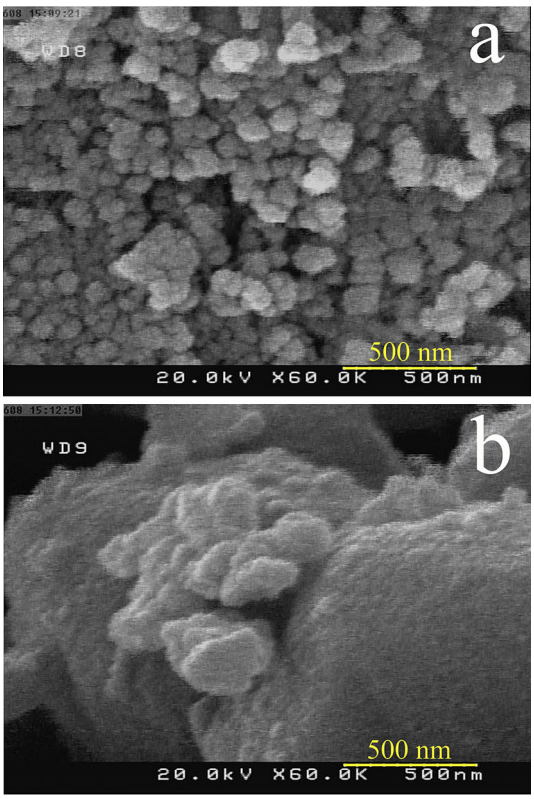

Fig. 7 FESEM images of the samples synthesized at **a** 25 and **b** 90 °C

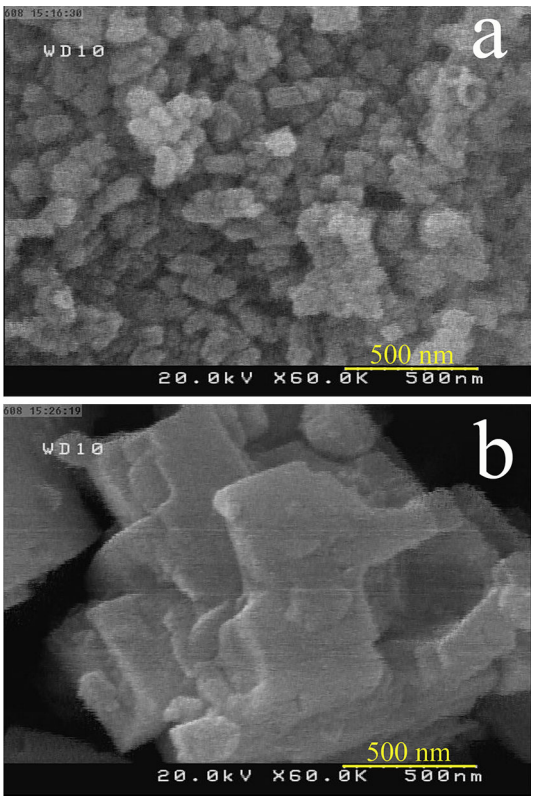

Fig. 8 FESEM images of the products prepared in presence of **a** SDS and **b** Titriplex III

and not uniform products. Maybe owing to employing the $Ba(Sal)_2$, there is no necessity to utilize any other surfactant sort. It seems that separated salicylaldehyde compound with the high steric hindrance influence from $Ba(Sal)_2$ in the reaction solution can act as capping agent to control the shape and size.

To examine the influence of the Ba source on the shape of the $BaSnO_3$, sample no. 10 was prepared with employing $Ba(NO_3)_2$ and $SnCl_2{\cdot}2H_2O$ in the presence of the TEPA at 60 °C (blank sample). Figure 9a exhibits FESEM image of the sample no. 9. It can be seen that bulk structures were obtained. The Sal ligand with high steric hindrance effect in $Ba(Sal)_2$, can play a capping agent role. It can be clearly observed that employing $Ba(Sal)_2$ as Ba source in presence of TEPA causes to prepare uniform spherical nanoparticles (Fig. 4c). Thus, the privilege of utilizing $Ba(Sal)_2$ is that it results in nanostructured $BaSnO_3$ preparation.

To examine the detailed morphology and size of the prepared $BaSnO_3$ sample in the optimum condition (sample no. 3) TEM analysis was performed. The TEM images (Fig. 9b, c) illustrate that quasi-spherical $BaSnO_3$ nanoparticles with diameter from 12 to 30 nm are sintered together. The high-resolution TEM (HRTEM) images of a single nanoparticle in Fig. 9d, e demonstrate that the nanoparticle is highly crystalline. The marked lattice fringes correspond to (110) plane in cubic phase of $BaSnO_3$ with a d-spacing of 0.291 nm.

It is generally accepted that the band gap (Eg) has a considerable impact on the detecting the characteristics of the nanometer-scale materials employed as photocatalyst and is frequently estimated from the UV–vis diffuse reflectance data. The UV–vis diffuse reflectance spectrum of the as-obtained $BaSnO_3$ nanostructures (sample no. 3) is illustrated in Fig. 10a. In this UV–vis diffuse reflectance spectrum, the absorption peak located at 354 nm. The (Eg) may be calculated based on the UV–vis diffuse reflectance data employing Tauc's equation [5]. The (Eg) of the $BaSnO_3$ as indirect semiconductor was estimated by extrapolating the linear section of the plot of $(\alpha h\nu)^{1/2}$ against $h\nu$ to the energy axis (Fig. 10b). The Eg value of the as-obtained nanostructured $BaSnO_3$ calculated to be

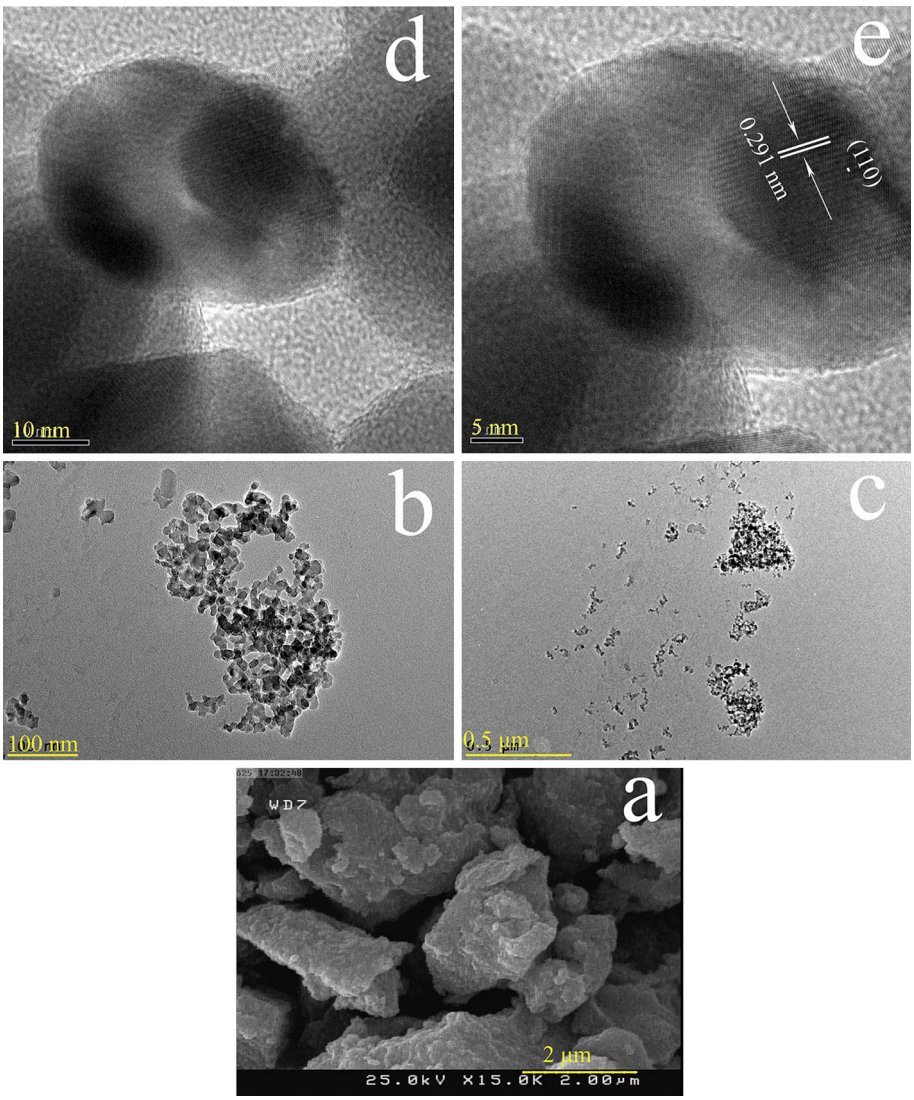

Fig. 9 FESEM image of sample no. 10 obtained from $Ba(NO_3)_2$ and $SnCl_2{\cdot}2H_2O$ via coprecipitation-calcination way (**a**) and TEM (**b**, **c**) and **d**, **e** HRTEM images of sample no. 3

3.37 eV. According to the obtained Eg value, as-prepared nanostructured $BaSnO_3$ sample can be employed as the photocatalyst.

Photodegradation of eriochrome black T (anionic dye) as water contaminant under UV light illumination was employed to evaluate the properties of the as-synthesized $BaSnO_3$ (sample no. 3). Figure 11 exhibits the obtained result. It has been reported that the Ba ions in the Ba containing ternary oxides play a key role for the photon polarization of the anionic subsystem [28]. No eriochrome black T was practically broken down after 120 min without employing UV light illumination or as-prepared nanostructured $BaSnO_3$. This observation illustrated that the contribution of self-degradation was insignificant. The proposed mechanism of the photocatalytic degradation of the eriochrome black T can be assumed as:

$$BaSnO_3 + h\nu \rightarrow BaSnO_3^* + e^- + h^+$$
$$h^+ + H_2O \rightarrow OH^{\cdot}$$
$$e^- + O_2 \rightarrow O_2^{-\cdot}$$
$$OH^{\cdot} + O_2^{-\cdot} + \text{eriochrome black T} \rightarrow \text{degradation products}$$

Utilizing photocatalytic calculations by Eq. (1), the eriochrome black T degradation was about 84 % after 120 min illumination of UV light. This obtained result demonstrates that as-prepared $BaSnO_3$ nanostructures have high potential to be applied as favorable and appropriate material for photocatalytic applications under illumination of UV light. The heterogeneous photocatalytic processes have diffusion, adsorption and reaction steps. It has been shown that the desirable distribution of the pore has effective and important impact on the diffusion of the

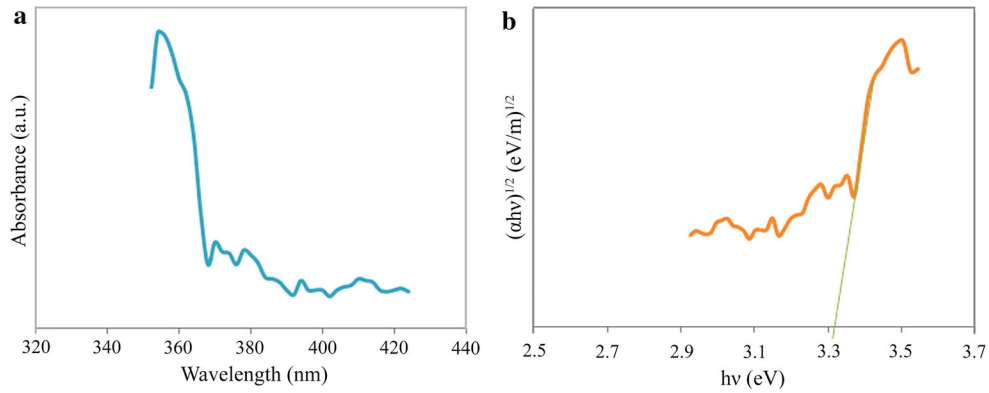

Fig. 10 UV-vis diffuse reflectance spectrum (**a**), plot to determine the band gap (**b**) of the $BaSnO_3$ nanostructures (sample no. 3)

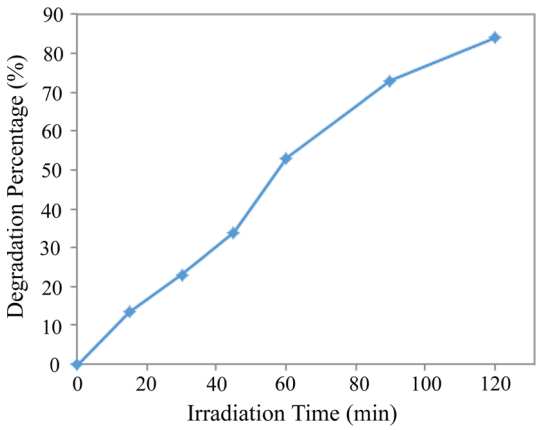

Fig. 11 Photocatalytic eriochrome black T degradation of $BaSnO_3$ nanostructures (sample no. 3) under UV light

reactants and products, and therefore effects on the photocatalytic activity. It seems that the enhanced photocatalytic activity of the as-obtained nanostructured $BaSnO_3$ can be owing to desirable and appropriate distribution of the pore, high hydroxyl amount and high separation rate of charge carriers [29–35] (Scheme 3).

4 Conclusions

A novel, reliable, facile and surfactant-free coprecipitation-calcination process has been developed to prepare pure barium stannate ($BaSnO_3$) nanostructures by employing $Ba(Sal)_2$ (Sal = salicylidene) and $SnCl_2{\cdot}2H_2O$ as precursors in presence of TEPA at 60 °C. To the best of our knowledge, it is the first time that $Ba(Sal)_2$ is employed as Ba source for the synthesis of the $BaSnO_3$ nanostructures. This investigation reveals that the $Ba(Sal)_2$ in presence of TEPA is an extremely good selection for uniform spherical $BaSnO_3$ nanostructures preparation without employing any surfactants. By changing the reaction temperature, precipitator and surfactant, we could obtain $BaSnO_3$ micro/nanostructures with various shapes and particle sizes. The as-obtained $BaSnO_3$ nanostructures can be employed as favorable and appropriate material for photocatalytic applications under illumination of UV light such as removal of eriochrome black T as anionic dye, since the eriochrome black T photodegradation percentage was found to be 84 within 120 min. FT-IR, XRD, and EDS analyses confirmed high purity of the as-prepared $BaSnO_3$.

Scheme 3 Reaction mechanism of eriochrome black T photodegradation over $BaSnO_3$ nanostructures under UV light irradiation

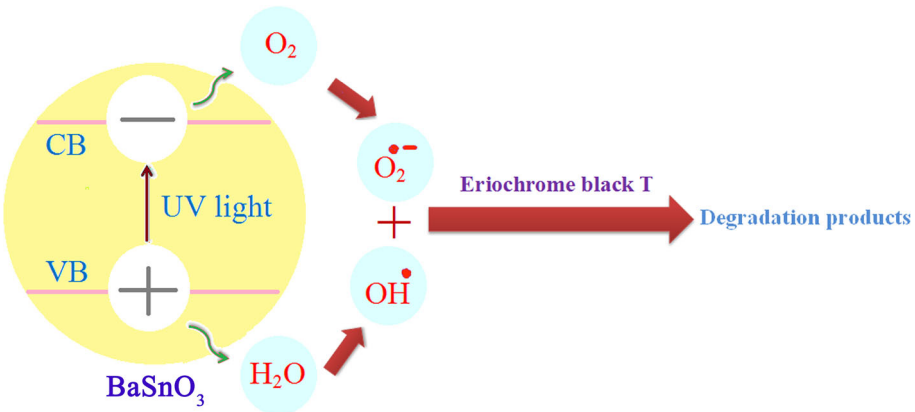

Acknowledgments The authors are grateful to University of Kashan for supporting this work by Grant No. 159271/20.

References

1. M. Sabet, M. Salavati-Niasari, Omid Amiri. Electrochim. Acta **117**, 504 (2014)
2. S. Mortazavi-Derazkola, S. Zinatloo-Ajabshir, M. Salavati-Niasari, Ceram. Int. **41**, 9593 (2015)
3. S. Zinatloo-Ajabshir, M. Salavati-Niasari, Int. J. Appl. Ceram. Technol. **11**, 654 (2014)
4. F. Beshkar, S. Zinatloo-Ajabshir, M. Salavati-Niasari, J. Mater. Sci.: Mater. Electron. **26**, 5043 (2015)
5. S. Zinatloo-Ajabshir, M. Salavati-Niasari, New J. Chem. **39**, 3948 (2015)
6. V.G. Wagner, H. Binder, Z. Anorg. Allg. Chem. **298**, 12 (1959)
7. Z. Zhigang, Z. Gang, Ferroelectrics **101**, 43 (1990)
8. P.H. Borse, J.S. Lee, H.G. Kim, J. Appl. Phys. **100**, 124915 (2006)
9. W. Wang, Sh Liang, K. Ding, J. Bi, J.C. Yu, P. Keung, L. Wong, J. Wu, J. Mater. Sci. **49**, 1893 (2014)
10. S.S. Shin, J.S. Kim, J.H. Suk, K.D. Lee, D.W. Kim, J.H. Park, I.S. Cho, K.S. Hong, J.Y. Kim, ACS Nano **7**, 1027 (2013)
11. J. Cerda, J. Arbiol, G. Dezanneau, R. Díaz, J.R. Morante, Sensors Actuators B **84**, 21 (2002)
12. T. Huang, T. Nakamura, M. Itoh, Y. Inaguma, O. Ishiyama, J. Mater. Sci. **30**, 1556 (1995)
13. W. Zhang, J. Tang, J. Ye, J. Mater. Res. **22**, 1859 (2007)
14. H. Mizoguchi, H.W. Eng, P.M. Woodward, Inorg. Chem. **43**, 1667 (2004)
15. V. Vorgelegt, L. Wensheng, Synthesis of nanosized $BaSnO_3$ powders. Doctoral thesis in Engineering of Natural Sciences, Faculty of Engineering, University of Saarlandes, Saarbrücken—Germany, 2002, pp. 1–2
16. S. Upadhyay, O. Parkash, D. Kumar, Mater. Lett. **49**, 251 (2001)
17. A.S. Deep, S. Vidya, P.C. Manu, S. Solomon, A. John, J.K. Thomas, J. Alloys Compd. **509**, 1830 (2011)
18. W. Lu, H. Schmidt, J. Sol-Gel. Sci. Technol. **42**, 55 (2007)
19. J. Ahmed, C.K. Blakely, S.R. Bruno, V.V. Poltavets, Mater. Res. Bull. **47**, 2282 (2012)
20. Y.H.O. Muñoz, M. Ponce, J. E. R. Páez Powder Technol. **279**, 86 (2015)
21. F. Beshkar, S. Zinatloo-Ajabshir, M. Salavati-Niasari, Chem. Eng. J. (2015). doi:10.1016/j.cej.2015.05.076
22. S. Zinatloo-Ajabshir, M. Salavati-Niasari, M. Hamadanian, RSC Adv. **5**, 33792 (2015)
23. S. Mortazavi-Derazkola, S. Zinatloo-Ajabshir, M. Salavati-Niasari, RSC Adv. **5**, 56666 (2015)
24. M. Shakouri-Arania, M. Salavati-Niasari, New J. Chem. **38**, 1179 (2014)
25. M. Ghaed-Amini, M. Bazarganipour, M. Salavati-Niasari, J. Ind. Eng. Chem. **21**, 1089 (2015)
26. G. Pfaff, V.D. Hildenbrand, H. Fuess, J. Mater. Sci. Lett. **17**, 1983 (1998)
27. S. Taoa, F. Gao, X. Liu, O. Toft Sùrensen. Sensors Actuators B **71**, 223 (2000)
28. B. Andriyevsky, A. Patryn, K. Dorywalski, Ch. Cobet, M. Piasecki, I. Kityk, N. Esser, T. Łukasiewicz, J. Dec, Ferroelectrics **426**, 194 (2012)
29. J. Zhong, J. Li, F. Feng, Y. Lu, J. Zeng, W. Hu, Z. Tang, J. Mol. Catal. A: Chem. **357**, 101 (2012)
30. D. Ghanbari, M. Salavati-Niasari, S. Karimzadeh, S. Gholamrezaei, J. NanoStruct. **4**, 227 (2014)
31. G. Nabiyouni, S. Sharifi, D. Ghanbari, M. Salavati-Niasari, J. NanoStruct. **4**, 317 (2014)
32. M. Panahi-Kalamuei, M. Mousavi-Kamazani, M. Salavati-Niasari, J. NanoStruct. **4**, 459 (2014)
33. F. Beshkar, M. Salavati-Niasari, J. NanoStruct. **5**, 17 (2015)
34. M. Goudarzi, D. Ghanbari, M. Salavati-Niasari, J. NanoStruct. **5**, 110 (2015)
35. S. Moshtaghi, M. Salavati-Niasari, D. Ghanbari, J. NanoStruct. **5**, 169 (2015)